ACS OMEGA

Article

Cite This: ACS Omega 2019, 4, 20844−20853

http://pubs.acs.org/journal/acsodf

Enhanced Adsorptive Desulfurization Using Mongolian Anthracite-Based Activated Carbon

Divyam Jha,[†] Mohd Belal Haider,[†] Rakesh Kumar,[†] Narandalai Byamba-Ochir,[‡] Wang Geun Shim,[§] Balathanigaimani Marriyappan Sivagnanam,*[,†] and Hee Moon*[,∥]

[†]Department of Chemical Engineering, Rajiv Gandhi Institute of Petroleum Technology, Jais 229304, India

[‡]Institute of Chemistry and Chemical Technology, Mongolian Academy of Sciences, Peace Avenue, Ulaanbaatar 13330, Mongolia

[§]Department of Polymer Science and Engineering, Sunchon National University, Suncheon-si, Jeollanam-do 57922, Republic of Korea

[∥]School of Chemical Engineering, Chonnam National University, 77 Yongbong-Ro, Buk-Gu, Gwangju 61186, Republic of Korea

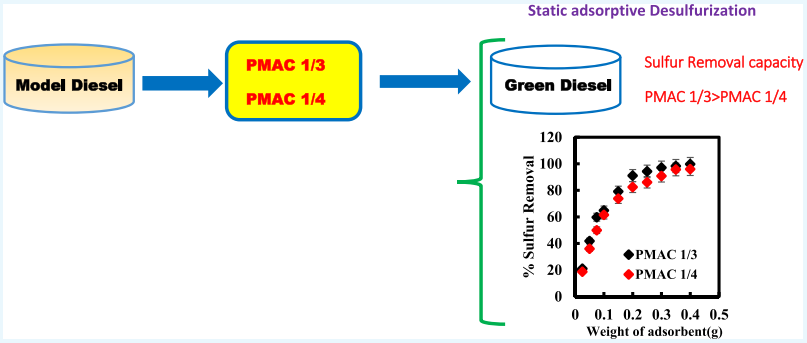

ABSTRACT: This study reports usage of Mongolian anthracite-based porous activated carbons (PMACs), namely, PMAC 1/3 and PMAC 1/4 for model diesel fuel desulfurization, having 500 ppmw of dibenzothiophene (DBT) in *n*-heptane. Further, the effects of contact time, adsorbent dosage, and temperature on the adsorption capacity were studied systematically. The experimental adsorption isotherm results were well represented by the Sips isotherm for PMAC 1/3 and the dual site Langmuir isotherm for PMAC 1/4. The maximum DBT adsorption by PMAC 1/3 and PMAC 1/4 were 99.7 and 95.7%, respectively. The kinetics for the adsorption of DBT on PMACs follows the pseudo second order behavior. The Weber−Morris plot shows the multilinearity over the entire time range, suggesting that both the surface and pore diffusions control the adsorption. The values of boundary layer thickness for PMAC 1/4 and PMAC 1/3 were found to be 3.183 and 1.643, respectively. Thus, PMAC 1/4 possesses more surface diffusion control than PMAC 1/3. The changes in Gibbs free energy (ΔG°), entropy (ΔS°), and enthalpy (ΔH°) are negative, which confirms that the studied process is spontaneous and exothermic and possesses less randomness at the interface. Based on the Sips isotherm, single-stage batch-adsorber design was prepared for the adsorption of DBT onto PMAC 1/3.

1. INTRODUCTION

The refractory sulfur compounds present in crude oil are becoming costlier for refiners worldwide. The increase of sulfur content in the crude oil and the strict norms on sulfur emission from diesel vehicles have made the desulfurization issue more serious.[1−4] The diesel sulfur content should be less than 10 ppm by 2020 as per the latest regulations in India. The major challenges for refineries in India are to meet the fuel sulfur specifications as well as reduce the aromatic content.[5,6]

Hydrodesulfurization (HDS) is a well-established process for desulfurization of liquid fuels.[7] However, it involves severe operating conditions and sensitive as well as most advanced catalysts to produce diesel with sulfur content less than 10 ppm, making the process expensive.[7,8] There are limitations for the HDS process to remove benzothiophene, dibenzothiophene (DBT), and alkyl substituent DBT.[9] Therefore, the other available desulfurization options involving oxidation, extraction, biochemical, and adsorption methods have been considered to produce ultralow-sulfur diesel to meet the new environmental regulations.[7−16] Among these methods, adsorptive desulfurization (ADS) has gained more attention because the adsorption technique is simple to operate and can be done even under ambient conditions. Various research groups have studied liquid-based ADS using different adsorbents.[16−22] The main challenge for the ADS process is to synthesize high adsorptive capacity adsorbents. In addition, adsorbents employed must possess thioselectivity for the heavy refractory sulfur compound adsorption that needs severe conditions to

Received: October 15, 2019
Accepted: November 12, 2019
Published: November 25, 2019

DOI: 10.1021/acsomega.9b03432
ACS Omega 2019, 4, 20844−20853

remove using the HDS process. In the past, several activated carbons (ACs) produced from coal and biomass were used.[16,23−25]

ACs are the most celebrated adsorbents for their application in separation and purification technologies because of their worthwhile surface properties.[26,27] ACs have also become very popular for ADS because of their microstructure.[23,28,29] The adsorption performance of ACs depends upon the adsorbent surface properties. In general, pore volume, specific surface area, pore size, and pore size distribution of an adsorbent play an important role in ADS.[26,30,31] However, the surface properties do not always have linear relation with the desulfurization capabilities[45] and therefore, to further enhance the adsorptive capabilities of adsorbents, researchers have impregnated ACs with metal halides.[26,28,32] In addition, it has been stated that the ADS performance of AC greatly depends on the precursor materials used and preparation methods.[33]

The carbon-rich, high bulk density Mongolian raw anthracite (MRA) with less ash content can be possibly used for producing adsorbents for ADS, as ACs from MRA have been already successfully tested for methane adsorption and capacitor applications.[34,35]

In the present study, novel Mongolian anthracite-based porous ACs (PMACs) were tested for sulfur removal from of the model diesel fuel (MDF) (DBT dissolved in *n*-heptane). It may be noted here that ADS using PMACs has not been reported yet according to the best of our knowledge. The adsorption results of DBT on PMAC 1/3 as well as PMAC 1/4 are presented in this report. The Sips, Langmuir, and dual site Langmuir isotherm models were used to study the equilibrium adsorption behavior of DBT on PMACs. The adsorption kinetics of DBT on PMACs was studied using the pseudo first order, pseudo second order, and diffusion models. Further, the thermodynamics of the adsorption system was investigated to determine the values of $\Delta H°$, $\Delta G°$, and $\Delta S°$. At last, a batch adsorption process design has also been proposed based on the results obtained.

2. EXPERIMENTAL

2.1. Materials. The method of preparation for the adsorbents PMAC 1/3 and PMAC 1/4 used in this study is given elsewhere.[35] The surface properties of the prepared PMACs are as follows: specific surface area (PMAC 1/3: 2038 m^2/g and PMAC 1/4: 2784 m^2/g), average pore volume (PMAC 1/3: 1.31 cm^3/g and PMAC 1/4: 2.27 cm^3/g), and average pore diameter (PMAC 1/3: 2.00 nm and PMAC 1/4: 2.20 nm).[35] The adsorbents were dried in a hot air oven at 110 °C for 12 h before every adsorption study. Beside these ACs, the chemicals used in this study, namely, DBT of purity >98% and *n*-heptane of purity >99% were purchased from Sigma-Aldrich Pvt ltd., India.

2.2. Model Diesel Fuel. For the preparation of the MDF, 0.1982 g of DBT was added into 100 mL of *n*-heptane as purchased without any further purification. The concentration of DBT is selected such that the total sulfur concentration should be 500 ppm by weight.

For investigating the selectivity of DBT over aromatic compounds, equimolar concentration of two polyaromatic hydrocarbons, namely, naphthalene and fluorene and one monoaromatic hydrocarbon, namely, ethylbenzene with different weight percentages (2, 4, 6, 8, and 10 wt %) were added into the MDF. The aromatic added MDFs were named MDF-A-α where α varies from 2 to 10 wt %. Because *n*-heptane has volatile nature; therefore, to avoid a change in the sulfur concentration, the prepared MDF was stored in amber vials.

2.3. Adsorption Equilibrium. The adsorption of DBT on PMACs was done at 30 °C and 250 rpm. In a typical experiment, 20 mL of MDF was taken in an Erlenmeyer flask with a known amount of the adsorbent (0.025−0.40 g). The mixture of MDF and the adsorbent was agitated in an Incubator shaker for 1 h. The DBT concentration in the desulfurized samples was analyzed by a gas chromatograph equipped with a flame ionization detector (PerkinElmer Claurs 580, GC-FID) after separating the adsorbent using a whatman paper. GC is equipped with a Elite-1 (length 50 m and inner diameter 200 μm) flame ionization detector as well.

The quantity adsorbed q_e (mg-S/g-A) was given by the eq 1 as below

$$q_e = (C_0 - C_e) \times \frac{V}{W} \tag{1}$$

where q_e is the quantity of sulfur adsorbed (mg-S/g-A), C_0 is the initial concentration of sulfur (mg-S/L-MDF), C_e is the equilibrium concentration of sulfur after the removal of sulfur by adsorption (mg-S/L-MDF). V and W are the volume of MDF (L) and W is mass (g) of the adsorbent, respectively. The percentage of sulfur removed was calculated using the following equation

$$\%\ \text{sulfur removal} = \frac{(C_0 - C_e)}{C_0} \times 100 \tag{2}$$

2.4. Data Analysis. To check the fitness accuracy of models, data analysis was done using the coefficient of determination (R^2), nonlinear error functions, residual root mean square error (RMSE), and chi-square test (χ^2). The empirical equations used for this study are as follows

$$R^2 = \frac{1 - \sum_{n=1}^{n} (q_{e,n} - q_{m,n})^2}{\sum_{n=1}^{n} (q_{e,n} - \overline{q_{e,n}})^2} \tag{3}$$

$$\text{RMSE} = \sqrt{\frac{1}{n-1} \sum_{n=1}^{n} (q_{e,n} - q_{m,n})^2} \tag{4}$$

$$\chi^2 = \sum_{n=1}^{n} \frac{(q_{e,n} - q_{m,n})^2}{q_{e,n}} \tag{5}$$

where q_e and q_m is the experimental and predicted value of the amount of sulfur adsorbed, respectively, and n is the number of observations. The data analysis was done based on the linear and nonlinear coefficient values. The R^2 value closer to unity and lower values of RMSE and χ^2 generally show that the predicted and experimental values fitted well. The average relative error (ARE) and normalized standard deviation (NSD) were employed to check the fitness of kinetic models. Generally, lower values of NSD and ARE indicate better model fitting. The equations for the calculation of NSD and ARE are given as follows

$$\text{NSD} = 100 \times \sqrt{\frac{1}{N-1} \sum_{i=1}^{N} \left[\frac{q_{t,e} - q_{t,m}}{q_{t,e}} \right]_i^2} \tag{6}$$

DOI: 10.1021/acsomega.9b03432
ACS Omega 2019, 4, 20844−20853

$$\mathrm{ARE} = \frac{100}{N}\sum_{i=1}^{N}\left[\frac{q_{t,e} - q_{t,m}}{q_{t,e}}\right]_i \quad (7)$$

where $q_{t,e}$ is the experimental and $q_{t,m}$ is the theoretically calculated quantity of sulfur adsorbed on PMACs.

3. RESULTS AND DISCUSSION

3.1. Effect of the Adsorbent Dosage. The removal capacity of sulfur was studied for different doses of adsorbents using MDF containing 500 ppm of total sulfur content. The dosage was taken in the range of 0.025−0.4 g of adsorbent for 20 mL of MDF as shown in Figure 1. Sulfur removal was

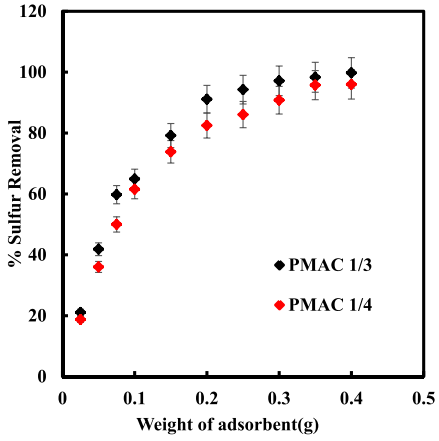

Figure 1. Effect of Adsorbent weight on sulfur removal at 303.15 K.

rigorously increased with increasing adsorbent weight from 0.025 to 0.25 g. Thereafter the removal efficiency has become constant for the adsorbent dose greater than 0.25 g for PMAC 1/3 and PMAC 1/4. The relative successive S-removal is small compared to removal with the initial adsorbent dosage. This shows that the equilibrium has been reached between the adsorbate and adsorbent under the operating conditions.[36] It shows the solid concentration effect or particles overcrowding.[37]

3.2. Equilibrium Isothermal Adsorption. The adsorption isothermal analysis was conducted using the MDF with a fixed initial sulfur concentration of 500 ppm and the adsorbent dosage varies from 2.5 to 40 g/l for 1 h at 30 °C. Figure 2 shows the relationship of the equilibrium amount of DBT adsorbed on the surface of PMAC 1/3 and PMAC 1/4 against equilibrium DBT concentration. As shown in Figure 2, q_e increases with C_e and reaches saturation which is the maximum adsorption capacity for PMAC 1/3 (~2.489 kmol/kg) and PMAC 1/4 to (~2.183 kmol/kg).

The observation of heterogeneity and homogeneity of the solid surface, calculation of adsorption energy, interaction between the fluid compound and solid phase adsorbent and the type of coverage were observed by the plot between C_e (kmol/m^3) versus q_e (kmol/kg). The increased adsorption is because of more surface area and adsorption sites with an increasing adsorbent quantity from 0.025 to 0.4 g.[38] The maximum DBT adsorption by PMAC 1/3 and PMAC 1/4 were 99.7 and 95.7%, respectively, as shown in Figure 1, for 0.4 g of the adsorbent in 60 min. The sample PMAC 1/3 showed relatively higher adsorptive capacity though PMAC 1/3 having a smaller surface area as compared to PMAC 1/4. The

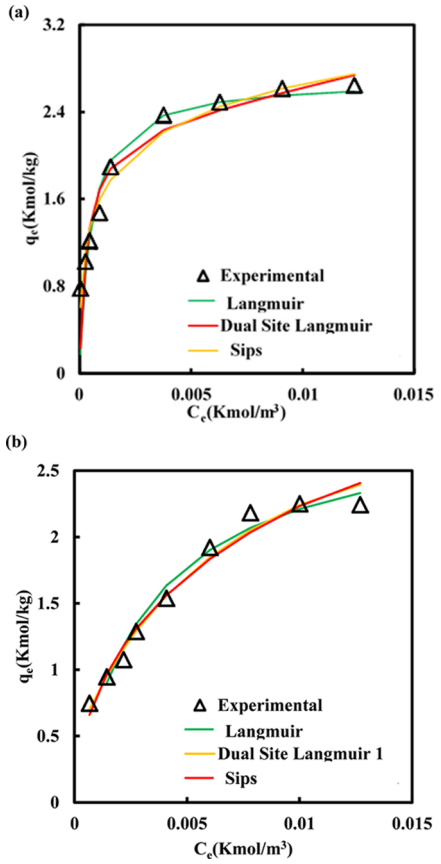

Figure 2. Adsorption isotherms of DBT on (a) PMAC 1/3 and (b) PMAC 1/4 at 303.15 K.

probable reason of higher removal using PMAC 1/3 could be its higher micropore volume fraction (66.4%) available as compared to PMAC 1/4 (42.2%). The DBT molecule size (0.8 nm)[39] is more closer to the pore diameter of PMAC 1/3 (2.0 nm)[35] than PMAC 1/4 (2.2 nm) which allows PMAC 1/3 to preferentially adsorb more DBT molecules.[37,40,41] Table 1 shows the ADS capabilities of various adsorbents. It can be observed that the adsorptive capacity of PMACs synthesized in this work have potential to adsorb the DBT molecule significantly.

3.3. Aspen Adsorption Isotherm Modelling. The DBT and *n*-heptane properties were evaluated by the Peng−Rob equation of state (PR-EOS) thermodynamic model. PR-EOS[42] is given as under

$$P = \frac{RT}{v - b} - \frac{a}{v(v + b) + b(v - b)} \quad (8)$$

where a and b are binary interaction parameters and depend on the critical properties as mentioned below

$$a = \frac{0.45724(RT_C)^2}{P_C}[1 + m(1 - T_r^{0.5})]^2 \quad (9)$$

$$b = 0.0778\frac{RT_C}{P_C} \quad (10)$$

3.3.1. Langmuir. In its formulation, Langmuir presumes monolayer adsorption that can only takes place at a finite number of definite localized, identical, and equivalent sites. These sites have no steric hindrance.[43,44] The Langmuir isotherm is given by the following equation

DOI: 10.1021/acsomega.9b03432
ACS Omega 2019, 4, 20844−20853

Table 1. DBT Adsorption Capacities of Different Adsorbents at Room Temperature

adsorbent	surface area (m^2/g)	adsorption time (min)	Adsorption capacity (mg/g)	initial sulfur content (ppm)	refs
microwave-synthesized carbon nanotubes	171.0	60	21.50	250	61
AC_{TD}	493.0	90	8.60	150	15
AC_{WS}	1570.0	30	47.10	220	62
ACFH-Cu^{+2}	1090.0	480	19.00	330	63
mesoporous carbon-silica nanocomposite via copper modification	276.0	2880	13.95	960	64
carbon aerogels	741.0	96	15.10	250	65
AC/γ-Fe_2O_3 nanocomposite	363.0	40	38.00		66
magnetic mesoporous carbon	705.0	60	62.00	1000	67
PMAC 1/3	2038.0	60	84.67	500	this work
PMAC 1/4	2784.0	60	74.97	500	this work

$$q_e = \frac{q_m K_a C_e}{1 + K_a C_e} \tag{12}$$

where q_e and q_m are sulfur adsorbed at equilibrium (mol-S/kg-A) and the maximum sulfur adsorbed at saturation (mol/kg). C_e is the equilibrium concentration of sulfur adsorbed (mol-S/L-M) and K_a is energy of adsorption.

3.3.2. Dual Site Langmuir. The dual site Langmuir model is used to describe the adsorption behavior on the heterogeneous adsorbent. The heterogeneous adsorbent is formed by two homogeneous sites with different energetic patches. If free energy of adsorbate−adsorbent on the patch is the same, the amount of adsorbed n is given as[45]

$$n = \left(\frac{n_1^s b_1 C}{1 + b_1 C}\right)_{site1} + \left(\frac{n_2^s b_2 C}{1 + b_2 C}\right)_{site2} \tag{13}$$

where n_1^s and n_2^s are the saturation capacities on site 1 and 2, respectively. b_1 and b_2 represent the affinity parameter of site 1 and 2, respectively, and C is the solute concentration. The assumptions for the Langmuir model are applicable at each patche. In addition, each site has different saturation capacities and the patches do not interact with each other.[46]

The free energy for two different sites is given as

$$b_j = b_{i0} \exp \frac{E_i}{RT} \tag{14}$$

where subscript i is the free-energy level of site 1 or 2, the pre-exponential factor of the component on site i is given by b_{i0} and E_i is the adsorption energy of the component on site i. The higher and lower adsorbate−adsorbent free energy is donated by, $i = 1$ and $i = 2$, respectively. For single gas adsorption, the free energy of site 1 is always greater than site 2.

3.3.3. Sips. Sips represents the limiting behavior of the Freundlich and Langmuir isotherms.[29] The Sips nonlinear equation model is described as

$$q_e = \frac{q_m b C_e^{1/n_s}}{1 + b C_e^{1/n_s}} \tag{15}$$

where n_s is the heterogeneity factor. If the value of n_s is greater than 1 then it is heterogeneous.[3] The Sips characteristics parameter is b and is in $(l/kmol)^{1/n_s}$.

All the isotherms were employed to analyze the adsorption equilibrium behavior of DBT on PMACs using Aspen Adsorption 8.4. The equilibrium adsorption data of DBT on PMAC 1/3 and PMAC 1/4 at 30 °C are shown in Figure 2. The goodness of fit of isotherm models with the experimental data was checked using the calculated values of χ^2 and RMSE,[28] which are given in Table 2. The data obtained from error analysis confirmed the best fit of Sips for PMAC 1/3 and dual site Langmuir for PMAC 1, respectively.

Table 2. Adsorption Isotherm Parameters

isotherms	aspen adsorption parameters	
	PMAC 1/3	PMAC 1/4
Langmuir	q_m = 2.701	q_m = 2.936
	K_a = 1890.620	K_a = 306.981
	R^2= 0.976	R^2= 0.960
	χ^2 = 2.124	χ^2 = 0.052
	RMSE = 0.027	RMSE = 0.003
dual site Langmuir	n_1 = 0.683	n_1 = 3.109
	$b_1 = 2.520 \times 10^{-4}$	$b_1 = 2.730 \times 10^{-3}$
	n_2 = 2.215	$n_2 = 4.410 \times 10^{-1}$
	$b_2 = 1.470 \times 10^{-3}$	$b_2 = 8.950 \times 10^{-2}$
	R^2= 0.968	R^2= 0.990
	χ^2 = 1.360	χ^2 = 0.014
	RMSE = 0.024	RMSE = 0.001
Sips	q_m = 4.629	q_m = 6.300
	b = 8.138	b = 7.602
	n_s = 0.390	n_s = 0.570
	R^2= 0.986	R^2= 0.975
	χ^2 = 0.101	χ^2 = 0.028
	RMSE = 0.007	RMSE = 0.002

3.4. Effect of Contact Time. The adsorbent size, the coefficient of diffusion, and the degree of mixing decides the quantity and rate at which the adsorbate adsorbs on the surface of the adsorbent.[47] MDF with DBT concentration 500 ppm were kept in contact with PMAC 1/3 and PMAC 1/4 for 2 g/l adsorbent amount at room temperature for 10−90 min. After 60 min a steady state was achieved and a quasi-equilibrium situation was obtained for both the adsorbents as shown in Figure 3. The adsorption rate rapidly increased in the earlier

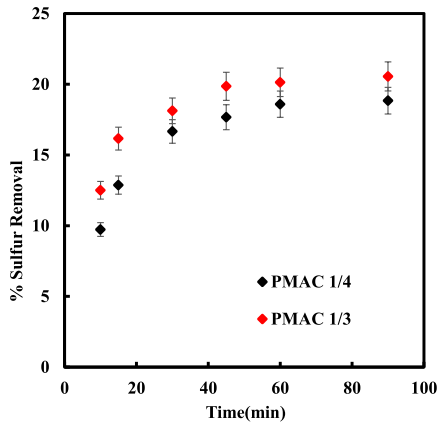

Figure 3. Effect of time on Sulfur removal at 303.15 K.

DOI: 10.1021/acsomega.9b03432
ACS Omega 2019, 4, 20844−20853

stage of experiments because of free sites available for adsorbates to adsorb on the surface. The initial fast adsorption depicts that the number of active sites available are more, and it slows down at equilibrium because of the few available sites and the mutual repulsive forces between the adsorbate present in the solution and at the surface of the adsorbent.[48]

3.5. Adsorption Kinetic Studies. The kinetic study is vital for designing an adsorption system. In the initial stage of adsorption meso- and macro-pores gets saturated with DBT molecules. Thereafter, the adsorption rate gets slowed down when the DBT molecules traverse further deep into the microspores and experience larger resistance in the later stage.[49] Thus, to get a better understanding of DBT adsorption on PMACs, pseudo first order and the second order models were used to obtain the kinetics data.

3.5.1. Pseudo First Order Kinetics. Pseudo first order kinetics assumes that DBT molecules are nondissociating on the surface of PMACs and no DBT molecule is present initially on the surface of the adsorbents PMAC 1/3 and PMAC 1/4. The pseudo first order kinetics is given by[50,51]

$$q_t = q_e(1 - e^{-k_1 t}) \tag{16}$$

where q_e, and q_t are sulfur adsorbed at equilibrium and at time t. k_1 (1/min) is the rate constant of pseudo first order adsorption.

3.5.2. Pseudo Second Order Kinetics. It is given by[52]

$$q_t = \frac{(k_2 q_e^{\,2} \cdot t)}{1 + (k_2 q_e \cdot t)} \tag{17}$$

The linear $\log(q_e - q_t)$ versus t was used for the pseudo first order kinetic model and the t/q_t versus t plot was used for the pseudo second order kinetic model as shown in Figure 4. The estimated kinetic parameters are given in Table 3. Lower values of ARE and NSD and higher values of R^2 values generally show the good fitting with the experimental data. It was observed that DBT removal by PMACs follows pseudo second order kinetics.

3.6. Diffusion Mechanism. The adsorbate transportation from bulk solution to the adsorbent surface may be controlled by single or multiple mechanisms,[53] that is, film or external diffusion, surface diffusion, pore diffusion, or a combination of two. The system controlled by film diffusion may have poor mixing, lower adsorbate concentration, small adsorbent particle size, and higher affinity between the adsorbate and adsorbent. Similarly, the intraparticle diffusion controls the system where the mixing is proper, high adsorbate concentration and lower affinity of the adsorbate for the adsorbent.[54]

$$B_t = -0.4977 - \ln(1 - F) \tag{18}$$

$$F = 1 - \frac{6}{\pi^2}\exp(-B_t) \tag{19}$$

where $F = q_t/q_e$ is the fraction of equilibrium attained, B_t is the function of F.

The diffusion mechanisms affecting the kinetics are given by Weber's intraparticle and Boyd's surface diffusion model.[55] The intraparticle diffusion-controlled mechanism is given by

$$q_t = k_{id} t^{1/2} + C \tag{20}$$

where K_{id} is the coefficient of intraparticle diffusion (mg/g(min)$^{0.5}$) and C depicts the boundary layer thickness

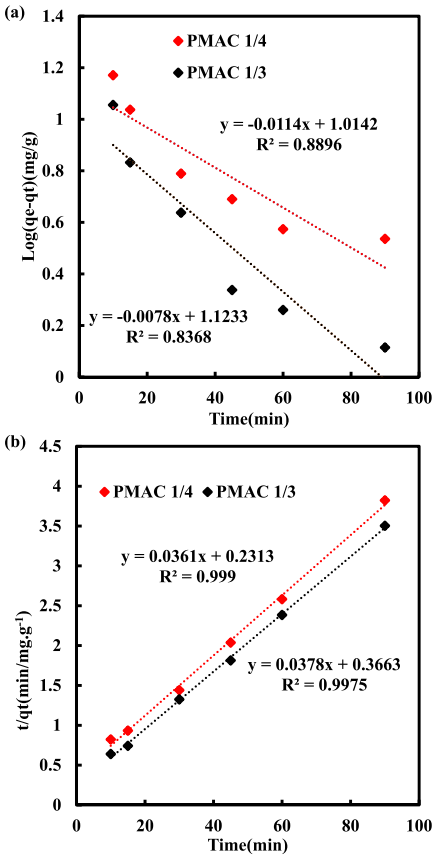

Figure 4. Kinetics for PMAC 1/4 and PMAC 1/3 (a) pseudo first order (b) pseudo second order kinetics at 303.15 K.

(boundary resistance). The surface diffusion controller mechanism is defined by Boyd's kinetic expression.[56]

The intercept and slope of the linear plot q_t versus $t^{0.5}$ given in Figure 5a are calculated to obtain the intraparticle diffusion coefficient K_{id} and boundary resistance C, respectively. If the overall adsorption data exhibit multilinear plots, then two or more steps control the diffusion. As shown in Figure 5a, PMAC 1/3 and PMAC 1/4 plots are not linear for the overall range; this concludes that one or more processes are influencing the adsorption. Hence, the adsorption process follows a complex mechanism, having both surface and intraparticle diffusion within the pores of PMAC 1/3 and PMAC 1/4.[57]

The initial and final linear portion shows the surface adsorption[58] and intraparticle diffusion effect,[47] respectively. The nearly parallel final segment of the plots suggests the comparability of adsorption rates for DBT into the PMAC pores at all temperatures. Further, to find the slowest step between intraparticle and surface diffusion, the Boyd kinetic model, eq 20, was used to further examine the kinetic data. The R^2 values of Boyd's plots given in Figure 5b, for both PMAC 1/3 and PMAC 1/4 confirms that the plot is linear. Thus, surface diffusion seems to be the rate-controlling step in the adsorption for both PMAC 1/3 and PMAC 1/4. The intercept values are given in Table 4. As given in the table the boundary layer thickness of PMAC 1/4 is greater than that of PMAC 1/3; thus, PMAC 1/4 is more surface diffusion controlled compared to PMAC 1/3. This conclusion is also well supported by the scanning electron microscopy (SEM) images of PMAC 1/3 and PMAC 1/4, as shown in Figure 6,

DOI: 10.1021/acsomega.9b03432
ACS Omega 2019, 4, 20844−20853

Table 3. Kinetics Parameters of Pseudo 1st and 2nd Order Models for the Adsorption of DBT on PMAC 1/3 and PMAC 1/4 at 303.15 K.

			Q_e (mg/g)									
			calculated	experimental	calculated	experimental	R^2	NSD	ARE	R^2	NSD	ARE
adsorbent	k_1 (1/min)	k_2 (g/mg min)	1st order		2nd order		1st order			2nd order		
PMAC 1/4	0.0262	0.156	2.76	23.55	27.70	23.55	0.89	28.15	31.11	0.99	0.42	0.07
PMAC 1/3	0.0179	0.103	3.07	25.69	26.45	25.69	0.84	19.77	18.03	0.99	0.08	1.12

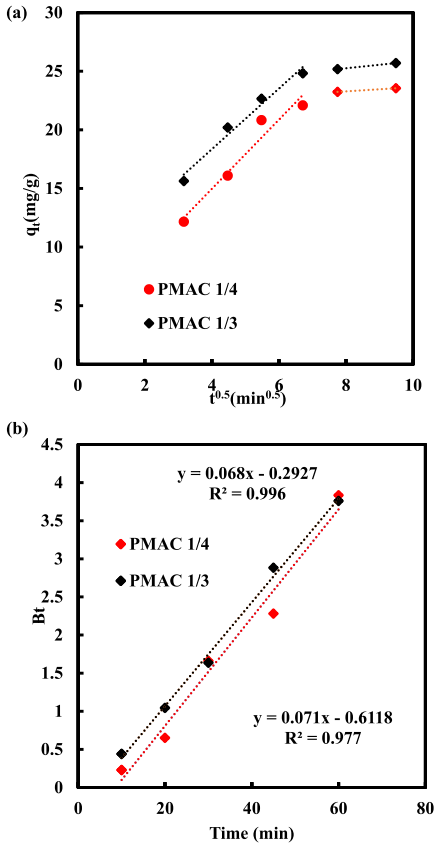

Figure 5. Intraparticle diffusion of DBT by (a) Weber and Morris Model (b) Boyd kinetic model for DBT adsorption.

Table 4. Intraparticle Diffusion Parameters for Adsorption of DBT on PMAC 1/3 and PMAC 1/4 by the Weber and Morris Model at 303.15 K

adsorbent	k_{id} (mg/g min$^{0.5}$)	C (mg/g)	R^2
PMAC 1/4	2.948	3.183	0.949
PMAC 1/3	2.586	1.643	0.999

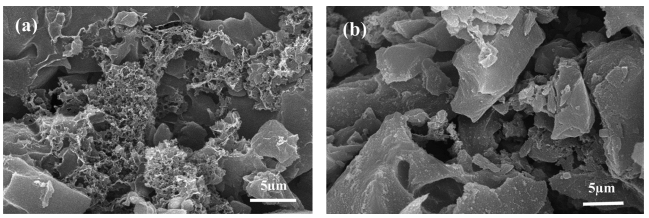

Figure 6. SEM images of (a) PMAC 1/3 and (b) PMAC 1/4.

PMAC 1/3 is more porous in nature and therefore, it has lower surface diffusion resistance for the DBT molecule to be adsorbed on the surface than PMAC 1/4. This result also explains the less pore diffusion-controlling mechanism for PMAC 1/3.

3.7. Thermodynamic Studies. The temperature effect on DBT adsorption on PMACs was studied as presented in Figure 7. It was found that with increasing temperature sulfur removal

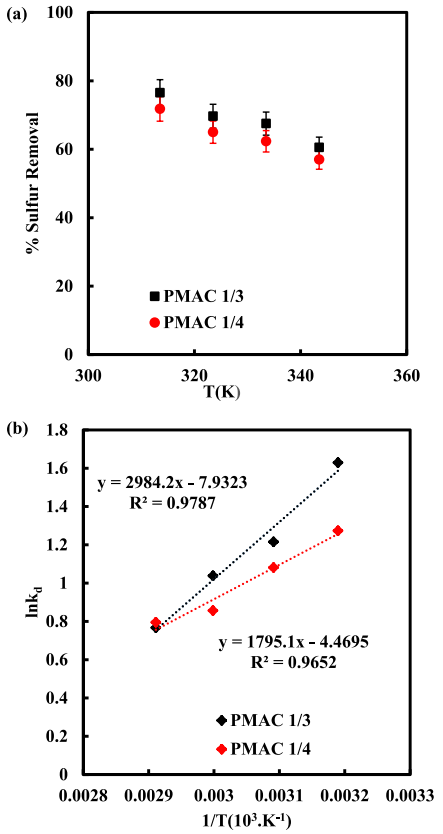

Figure 7. (a) Effect of temperature on DBT adsorption on PMAC 1/3 and PMAC 1/4 (b) modelling for thermodynamic behavior of DBT on PMAC 1/3 and PMAC 1/4 using Van't Hoff equation.

decreases as shown Figure 7a. The reduction in adsorption of DBT on PMACs with increase in temperature shows that the adsorption is following physisorption phenomena. The ΔG° was calculated by using eq 21 whereas ΔS° and ΔH° were determined from the intercept and slope of the linear Van't Hoff plot between ln K_d and $1/T$ as shown in Figure 7b, which depicts the thermodynamic behavior of the adsorption process. The ΔG° was evaluated by the given equation

$$\Delta G^\circ = -RT \ln K_d \tag{21}$$

$$K_d = \frac{\text{DBT concentration adsorbed}}{\text{DBT concentration remained in the solution}}$$

where ΔG° is the change is Gibb's free energy, K_d is the distribution coefficient, R is the gas constant and T is

DOI: 10.1021/acsomega.9b03432
ACS Omega 2019, 4, 20844−20853

Table 5. Thermodynamic Parameters for the Adsorption of DBT on PMAC 1/3 and PMAC 1/4

	K_d		$\Delta G°$ (Kcal/mol)		$\Delta H°$ (Kcal/mol)		$\Delta S°$ [Kcal/(mol. K)]	
T (C)	PMAC 1/3	PMAC 1/4	PMAC 1/3	PMAC 1/4	PMAC 1/3	PMAC 1/4	PMAC 1/3	PMAC 1/4
40	5.099	3.572	−4.244	−3.317	−14.890	−0.037	−24.760	−0.065
50	3.372	2.948	−3.267	−2.907				
60	2.825	2.354	−2.877	−2.372				
70	2.153	2.214	−2.189	−2.269				

temperature in K. The Van't Hoff equation was used to calculate the $\Delta H°$ and change in entropy $\Delta S°$

$$\ln K_d = \left(\frac{\Delta S°}{R}\right) - \left(\frac{\Delta H°}{RT}\right) \quad (22)$$

Thermodynamic parameters of the system are shown in Table 5. The negative $\Delta G°$ value confirms spontaneity and feasibility of the system.[45] The negative values of $\Delta H°$ confirm that the overall adsorption process is exothermic in nature. Negative $\Delta S°$ values indicate the decrease in the degree of freedom of the adsorbed DBT molecule on PMACs.[48−50]

3.8. Design of Batch Sorption from Isotherm Data. The single-stage batch adsorption system can be designed using the adsorption isotherm.[44,54,59,60] A schematic diagram is shown in Figure 8 considering the volume of MDF, V (L); the DBT concentration reduces from C_0 to C_1 (mg/L), the DBT loading changes from q_0 to q_1 (mg/g), and the amount of adsorbent is M (mg). At time $t = 0$, $q_0 = 0$ and as time passes the mass balance equates DBT removed from the MDF to that picked up by the solid. The mass balance equation for the system shown in Figure 8a is

$$V(C_0 - C_1) = M(q_0 - q_1) = Mq_1 \quad (23)$$

Under equilibrium conditions $C_1 \rightarrow C_e$ $q_1 \rightarrow q_e$

Because the Sips isotherm fits the equilibrium data for DBT onto PMAC 1/3, the Sips isotherm equation can be used to modify the batch adsorber design equation as presented below

$$\frac{M}{V} = \frac{(C_0 - C_e)}{q_1} = \frac{(C_0 - C_e)}{q_e} = \frac{C_0 - C_e}{\frac{q_m b C_e^{1/n_s}}{1 + b C_e^{1/n_s}}} \quad (24)$$

Figure 8b shows the plot between the predicted amount of PMAC 1/3 needed to remove different percentages of DBT from the MDF of initial concentrations 500 mg/L at different solution volumes. The design procedure is defined for a single-stage batch sorption system. For example, the quantity of PMAC 1/3 required for the 90% removal of DBT from the MDF of concentration 500 mg/L was 97.21, 194.43, 291.64, and 388.84 mg for MDF volumes of 1, 2, 3, and 4 L, respectively.

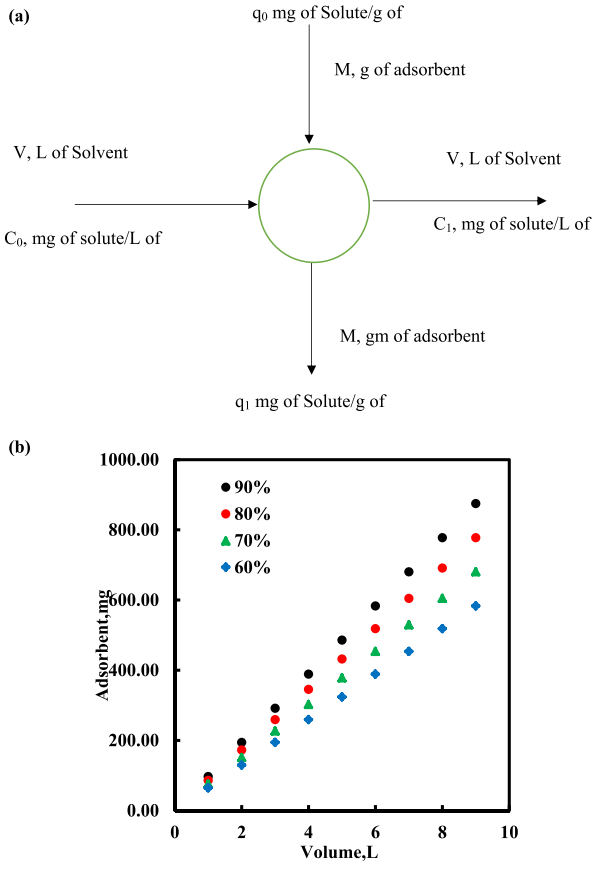

Figure 8. (a) Single-stage batch-adsorber design for PMAC 1/3 (b) adsorbent mass (M) against volume of solution treated (L) at 303.15 K.

3.9. Effect of Aromatics on DBT Removal. It is a well-known fact that the aromatic compounds present in diesel generally compete with the sulfur-bearing compounds to occupy the adsorption sites of most of the adsorbents. Therefore, further study was conducted to investigate the effect of aromatics present in MDF-A-α on DBT adsorption. The effect of aromatics present in the MDF-A-α is shown in Figure 9. It can be observed from the figure that the adsorption of aromatic compounds increases with increasing the dosage of the adsorbent. The highest adsorption after DBT is shown by fluorine followed by naphthalene and ethylbenzene. The results show that both adsorbents have affinity for the aromatic compounds which may inhibit the sulfur removal capacity of the adsorbent. To understand the inhibiting effect of aromatics, different weight % of the aromatics was used and their effect on sulfur removal was examined as shown in Figure 10. It was noted that the increasing aromatic concentration negatively impacted the sulfur uptake of the adsorbents. This arises because of competitive adsorption between DBT and the aromatics resulting in decrease in sulfur uptake. Similar to the results of sulfur removal from the MDF using PMACs 1/3 and 1/4, PMAC 1/3 shows better performance for the removal of sulfur from MDF-A-α.

4. CONCLUSIONS

In this work, DBT adsorption capacity of PMACs has been studied. The study shows that the desulfurization ability of PMAC 1/3 (84.56 mg/g) exhibits better performance compared to PMAC 1/4 (74.25 mg/g). The higher desulfurization capabilities of PMAC 1/3 have direct correspondence with the better microporosity. PMAC 1/3 follows Sips and PMAC 1/4 follows the dual site Langmuir

DOI: 10.1021/acsomega.9b03432
ACS Omega 2019, 4, 20844−20853

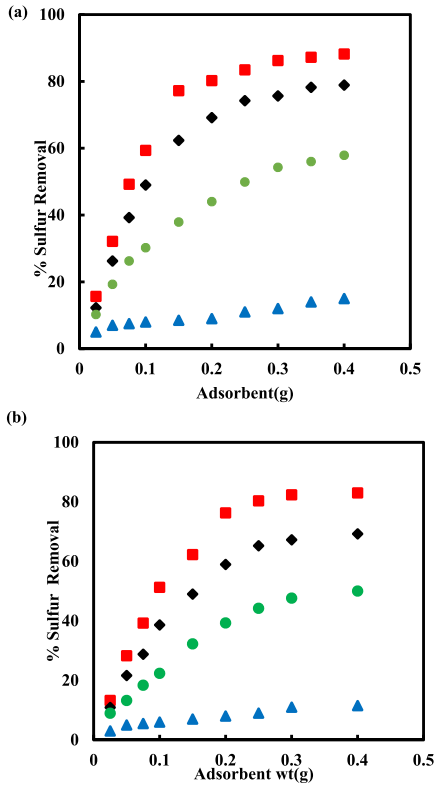

Figure 9. Effect on adsorption of DBT, fluorene, naphthalene, and ethyl benzene present in the MDF-A-α with a change in the adsorbent weight (A) PMAC_1/3 (B) PMAC_1/4.

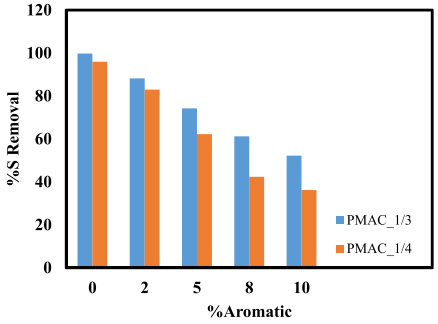

Figure 10. Effect of aromatics concentration on sulfur adsorption capacity.

adsorption isotherms model. The diffusion of DBT in PMACs follows a complex diffusion model which means both intraparticle and surface diffusions. In addition, DBT adsorption on PMACs follows pseudo second order kinetics. The thermodynamic studies revealed that the adsorption of DBT on PMACs is an exothermic and spontaneous process having less randomness at the interface. Further, the present study significantly indicates that the aromatics affects the adsorption of DBT on the PMACs.

AUTHOR INFORMATION

Corresponding Authors

*E-mail: msbala@rgipt.ac.in (B.M.S.).
*E-mail: hmoon@chonnam.ac.kr (H.M.).

ORCID

Divyam Jha: 0000-0001-7303-8913
Mohd Belal Haider: 0000-0002-3228-391X
Rakesh Kumar: 0000-0001-9926-6156

Notes

The authors declare no competing financial interest.

ACKNOWLEDGMENTS

The research work was funded by Rajiv Gandhi Institute of Petroleum Technology (RGIPT), Jais.

REFERENCES

(1) Song, C. An Overview of New Approaches to Deep Desulfurization for Ultra-Clean Gasoline, Diesel Fuel and Jet Fuel. *Catal. Today* **2003**, *86*, 211−263.
(2) Babich, I. V.; Moulijn, J. A. 03/02171 Science and Technology of Novel Processes for Deep Desulfurization of Oil Refinery Streams: A Review. *Fuel* **2003**, *82*, 607−631; *Fuel Energy Abstr.* **2003**, *44*, 362.
(3) Sentorun-Shalaby, C.; Saha, S. K.; Ma, X.; Song, C. Mesoporous-Molecular-Sieve-Supported Nickel Sorbents for Adsorptive Desulfurization of Commercial Ultra-Low-Sulfur Diesel Fuel. *Appl. Catal. B Environ.* **2011**, *101*, 718−726.
(4) Song, C.; Ma, X. New Design Approaches to Ultra-Clean Diesel Fuels by Deep Desulfurization and Deep Dearomatization. *Appl. Catal. B Environ.* **2003**, *41*, 207−238.
(5) Ma, X.; Velu, S.; Kim, J. H.; Song, C. Deep Desulfurization of Gasoline by Selective Adsorption over Solid Adsorbents and Impact of Analytical Methods on Ppm-Level Sulfur Quantification for Fuel Cell Applications. *Appl. Catal. B Environ.* **2005**, *56*, 137−147.
(6) Ma, X.; Sprague, M.; Song, C. Deep Desulfurization of Liquid Hydrocarbons by Selective Adsorption for Fuel Cell Applications. *ACS Div. Pet. Chem. Inc. Prepr.* **2002**, *47*, 48−49.
(7) Kim, B. H.; Kim, H. Y.; Kim, T. S.; Park, D. H. Selectivity of Desulfurization Activity of Desulfovibrio Desulfuricans M6 on Different Petroleum Products. *Fuel Process. Technol.* **1995**, *43*, 87−94.
(8) Kim, H.; Lee, J. J.; Moon, S. H. Hydrodesulfurization of Dibenzothiophene Compounds Using Fluorinated NiMo/Al2O3 Catalysts. *Appl. Catal. B Environ.* **2003**, *44*, 287−299.
(9) Saleh, T. A.; Sulaiman, K. O.; AL-Hammadi, S. A. Effect of Carbon on the Hydrodesulfurization Activity of MoCo Catalysts Supported on Zeolite/Active Carbon Hybrid Supports. *Appl. Catal. B Environ.* **2019**, 117661.
(10) Gray, K. A.; Mrachko, G. T.; Squires, C. H. Biodesulfurization of Fossil Fuels. *Curr. Opin. Microbiol.* **2003**, *6*, 229−235.
(11) Shan, G.; Liu, H.; Xing, J.; Zhang, G.; Wang, K. Separation of Polycyclic Aromatic Compounds from Model Gasoline by Magnetic Alumina Sorbent Based on π-Complexation. *Ind. Eng. Chem. Res.* **2004**, *43*, 758−761.
(12) Saleh, T. A.; Siddiqui, M. N.; Al-Arfaj, A. A. Synthesis of Multiwalled Carbon Nanotubes-Titania Nanomaterial for Desulfurization of Model Fuel. *J. Nanomater.* **2014**, *2014*, 1.
(13) Saleh, T. A.; Danmaliki, G. I. Influence of Acidic and Basic Treatments of Activated Carbon Derived from Waste Rubber Tires on Adsorptive Desulfurization of Thiophenes. *J. Taiwan Inst. Chem. Eng.* **2016**, *60*, 460−468.
(14) Saleh, T. A.; Sulaiman, K. O.; AL-Hammadi, S. A.; Dafalla, H.; Danmaliki, G. I. Adsorptive Desulfurization of Thiophene, Benzothiophene and Dibenzothiophene over Activated Carbon Manganese Oxide Nanocomposite: With Column System Evaluation. *J. Clean. Prod.* **2017**, *154*, 401−412.
(15) Saleh, T. A.; Danmaliki, G. I. Adsorptive Desulfurization of Dibenzothiophene from Fuels by Rubber Tyres-Derived Carbons: Kinetics and Isotherms Evaluation. *Process Saf. Environ. Prot.* **2016**, *102*, 9−19.
(16) Yu, G.; Lu, S.; Chen, H.; Zhu, Z. Diesel Fuel Desulfurization with Hydrogen Peroxide Promoted by Formic Acid and Catalyzed by Activated Carbon. *Carbon* **2005**, *43*, 2285−2294.
(17) Weitkamp, J.; Schwark, M.; Ernst, S. Removal of Thiophene Impurities from Benzene. *J. Chem. Soc., Chem. Commun.* **1991**, 1133−1134.

DOI: 10.1021/acsomega.9b03432
ACS Omega 2019, 4, 20844−20853

(18) Lee, S. H. D.; Kumar, R.; Krumpelt, M. Sulfur Removal from Diesel Fuel-Contaminated Methanol. *Sep. Purif. Technol.* **2002**, *26*, 247−258.
(19) Ma, X.; Sun, L.; Song, C. A New Approach to Deep Desulfurization of Gasoline, Diesel Fuel and Jet Fuel by Selective Adsorption for Ultra-Clean Fuels and for Fuel Cell Applications. *Catal. Today* **2002**, *77*, 107−116.
(20) Hernández-Maldonado, A. J.; Stamatis, S. D.; Yang, R. T.; He, A. Z.; Cannella, W. New Sorbents for Desulfurization of Diesel Fuels via π Complexation: Layered Beds and Regeneration. *Ind. Eng. Chem. Res.* **2004**, *43*, 769−776.
(21) Sano, Y.; Sugahara, K.; Choi, K.; Korai, Y.; Mochida, I. Two-Step Adsorption Process for Deep Desulfurization of Diesel Oil. *Fuel* **2005**, *84*, 903−910.
(22) Li, W.; Liu, Q.; Xing, J.; Gao, H.; Xiong, X.; Li, Y.; Li, X. High-Efficiency Desulfurization by Adsorption with Mesoporous Aluminosilicates Wangliang. *AIChE J.* **2007**, *53*, 3263−3268.
(23) Seredych, M.; Lison, J.; Jans, U.; Bandosz, T. J. Textural and Chemical Factors Affecting Adsorption Capacity of Activated Carbon in Highly Efficient Desulfurization of Diesel Fuel. *Carbon* **2009**, *47*, 2491−2500.
(24) Marín-Rosas, C.; Ramírez-Verduzco, L. F.; Murrieta-Guevara, F. R.; Hernández-Tapia, G.; Rodríguez-Otal, L. M. Desulfurization of Low Sulfur Diesel by Adsorption Using Activated Carbon: Adsorption Isotherms. *Ind. Eng. Chem. Res.* **2010**, *49*, 4372−4376.
(25) Yu, C.; Qiu, J. S.; Sun, Y. F.; Li, X. H.; Chen, G.; Zhao, Z. B. Adsorption Removal of Thiophene and Dibenzothiophene from Oils with Activated Carbon as Adsorbent: Effect of Surface Chemistry. *J. Porous Mater.* **2008**, *15*, 151−157.
(26) Jeon, H.-J.; Ko, C. H.; Kim, S. H.; Kim, J.-N. Removal of Refractory Sulfur Compounds in Diesel Using Activated Carbon with Controlled Porosity. *Energy Fuel.* **2009**, *23*, 2537−2543.
(27) Muzic, M.; Sertic-Bionda, K.; Gomzi, Z. Kinetic and Statistical Studies of Adsorptive Desulfurization of Diesel Fuel on Commercial Activated Carbons. *Chem. Eng. Technol.* **2008**, *31*, 355−364.
(28) Wang, Y.; Yang, R. T. Desulfurization of Liquid Fuels by Adsorption on Carbon-Based Sorbents and Ultrasound-Assisted Sorbent Regeneration. *Langmuir* **2007**, *23*, 3825−3831.
(29) Wen, J.; Han, X.; Lin, H.; Zheng, Y.; Chu, W. A Critical Study on the Adsorption of Heterocyclic Sulfur and Nitrogen Compounds by Activated Carbon: Equilibrium, Kinetics and Thermodynamics. *Chem. Eng. J.* **2010**, *164*, 29−36.
(30) Selvavathi, V.; Chidambaram, V.; Meenakshisundaram, A.; Sairam, B.; Sivasankar, B. Adsorptive Desulfurization of Diesel on Activated Carbon and Nickel Supported Systems. *Catal. Today* **2009**, *141*, 99−102.
(31) Kim, J. H.; Ma, X.; Zhou, A.; Song, C. Ultra-Deep Desulfurization and Denitrogenation of Diesel Fuel by Selective Adsorption over Three Different Adsorbents: A Study on Adsorptive Selectivity and Mechanism. *Catal. Today* **2006**, *111*, 74−83.
(32) Zhou, A.; Ma, X.; Song, C. Liquid-Phase Adsorption of Multi-Ring Thiophenic Sulfur Compounds on Carbon Materials with Different Surface Properties. *J. Phys. Chem. B* **2006**, *110*, 4699−4707.
(33) Bu, J.; Loh, G.; Gwie, C. G.; Dewiyanti, S.; Tasrif, M.; Borgna, A. Desulfurization of Diesel Fuels by Selective Adsorption on Activated Carbons: Competitive Adsorption of Polycyclic Aromatic Sulfur Heterocycles and Polycyclic Aromatic Hydrocarbons. *Chem. Eng. J.* **2011**, *166*, 207−217.
(34) Byamba-Ochir, N.; Shim, W. G.; Balathanigaimani, M. S.; Moon, H. High Density Mongolian Anthracite Based Porous Carbon Monoliths for Methane Storage by Adsorption. *Appl. Energy* **2017**, *190*, 257−265.
(35) Lee, H.-C.; Byamba-Ochir, N.; Shim, W.-G.; Balathanigaimani, M. S.; Moon, H. High-Performance Super Capacitors Based on Activated Anthracite with Controlled Porosity. *J. Power Sources* **2015**, *275*, 668−674.
(36) Davis, B. Effect o f PP % on Crystal Phase o f Zd32 Precipitated from Solution and Calcined at 600 ° C. *J. Am. Ceram. Soc.* **1984**, *14*, 1983.
(37) Jolly, S. C. Meat Extract. *Official Standardized and Recommendation Methods of Analysis*; The Society for Analytical Chemistry, 1963; 130. 1963.
(38) Kumar, S.; Srivastava, V. C.; Badoni, R. P. Studies on Adsorptive Desulfurization by Zirconia Based Adsorbents. *Fuel* **2011**, *90*, 3209−3216.
(39) Bamufleh, H. Adsorption of Dibenzothiophene (DBT) on Activated Carbon from Dates' Stones Using Phosphoric Acid (H_3PO_4). *JKAU Eng. Sci* **2011**, *22*, 89−105.
(40) Nazal, M. K.; Khaled, M.; Atieh, M. A.; Aljundi, I. H.; Oweimreen, G. A.; Abulkibash, A. M. The Nature and Kinetics of the Adsorption of Dibenzothiophene in Model Diesel Fuel on Carbonaceous Materials Loaded with Aluminum Oxide Particles. *Arabian J. Chem.* **2015**, DOI: 10.1016/j.arabjc.2015.12.003.
(41) Hu, J. *Advanced Materials and Structural Engineering*; CRC Press, 2015; pp 57−60.
(42) Jaubert, J.-N.; Mutelet, F. VLE Predictions with the Peng-Robinson Equation of State and Temperature Dependent Kij Calculated through a Group Contribution Method. *Fluid Phase Equilib.* **2004**, *224*, 285−304.
(43) Foo, K. Y.; Hameed, B. H. Insights into the Modeling of Adsorption Isotherm Systems. *Chem. Eng. J.* **2010**, *156*, 2−10.
(44) Zhang, Y.; Yang, Y.; Han, H.; Yang, M.; Wang, L.; Zhang, Y.; Jiang, Z.; Li, C. Ultra-Deep Desulfurization via Reactive Adsorption on Ni/ZnO: The Effect of ZnO Particle Size on the Adsorption Performance. *Appl. Catal. B Environ.* **2010**, *19*, 327−332.
(45) Ritter, J. A.; Bhadra, S. J.; Ebner, A. D. On the Use of the Dual-Process Langmuir Model for Correlating Unary Equilibria and Predicting Mixed-Gas Adsorption Equilibria. *Langmuir* **2011**, *27*, 4700−4712.
(46) Langmuir, I. *Equação de Langmuir*, 1918; p 345, (1914).
(47) Nsami, N. J.; Ketcha, M. J. The Adsorption Efficiency of Chemically Prepared Activated Carbon from Cola Nut Shells by $ZnCl_2$ on Methylene Blue. *J. Chem.* **2013**, *2013*, 1−7.
(48) Zhao, W.; Zhu, J.; Wei, W.; Ma, L.; Zhu, J.; Xie, J. Comparative Study of Modified/Non-Modified Aluminum and Silica Aerogels for Anionic Dye Adsorption Performance. *RSC Adv.* **2018**, *8*, 29129−29140.
(49) Suresh, S.; Srivastava, V. C.; Mishra, I. M. Studies of Adsorption Kinetics and Regeneration of Aniline, Phenol, 4-Chlorophenol and 4-Nitrophenol by Activated Carbon. *Chem. Ind. Chem. Eng. Q.* **2012**, *19*, 195−212.
(50) Lagergren, S. About the Theory of So-Called Adsorption of Soluble Substances. *K. Sven. Vetenskapsakad. Handl.* **1898**, *24*, 1.
(51) Ishaq, M.; Sultan, S.; Ahmad, I.; Ullah, H.; Yaseen, M.; Amir, A. Adsorptive Desulfurization of Model Oil Using Untreated, Acid Activated and Magnetite Nanoparticle Loaded Bentonite as Adsorbent. *J. Saudi Chem. Soc.* **2017**, *21*, 143−151.
(52) Ho, Y. S.; McKay, G. Comparative Sorption Kinetic Studies of Dye and Aromatic Compounds onto Fly Ash. *J. Environ. Sci. Health, Part A: Toxic/Hazard. Subst. Environ. Eng.* **1999**, *34*, 1179−1204.
(53) Ahmed, M. J. K.; Ahmaruzzaman, M. Adsorptive Desulfurization of Feed Diesel Using Chemically Impregnated Coconut Coir Waste. *Int. J. Environ. Sci. Technol.* **2015**, *12*, 2847−2856.
(54) Aravindhan, R.; Rao, J. R.; Nair, B. U. Removal of Basic Yellow Dye from Aqueous Solution by Sorption on Green Alga Caulerpa Scalpelliformis. *J. Hazard. Mater.* **2007**, *142*, 68−76.
(55) Weber, W. J., Jr.; Morris, J. C. Kinetics of Adsorption on Carbon from Solution. *J. Sanit. Eng. Div.* **1963**, *89*, 31−59.
(56) Boyd, G. E.; Adamson, A. W. The Exchange Adsorption of Ions from Aqueous Solutions by Organic Zeolites. 11. Kinetics. *J. Am. Chem. Soc.* **1947**, *69*, 2836.
(57) Ofomaja, A. E. Intraparticle Diffusion Process for Lead(II) Biosorption onto Mansonia Wood Sawdust. *Bioresour. Technol.* **2010**, *101*, 5868−5876.
(58) Srivastav, A.; Srivastava, V. C. Adsorptive Desulfurization by Activated Alumina. *J. Hazard. Mater.* **2009**, *170*, 1133−1140.

DOI: 10.1021/acsomega.9b03432
ACS Omega 2019, 4, 20844−20853

(59) Dŏgan, M. A. M.; Alkan, M.; Onganer, Y. Adsorption of Methylene Blue From Aqueous Solution Onto Perlite. *Water, Air, Soil Pollut.* **2000**, *120*, 229−248.
(60) Crittenden, B.; Thomas, W. J. *Adsorption Technology and Design Technology*; Butterworth-Heinemann, 1998; p 288.
(61) Jha, D.; Mubarak, N. M.; Haider, M. B.; Kumar, R.; Balathanigaimani, M. S.; Sahu, J. N. Adsorptive Removal of Dibenzothiophene from Diesel Fuel Using Microwave Synthesized Carbon Nanomaterials. *Fuel* **2019**, *244*, 132−139.
(62) Yang, Y.; Lu, H.; Ying, P.; Jiang, Z.; Li, C. Selective Dibenzothiophene Adsorption on Modified Activated Carbons. *Carbon* **2007**, *45*, 3042−3044.
(63) Moosavi, E. S.; Dastgheib, S. A.; Karimzadeh, R. Adsorption of Thiophenic Compounds from Model Diesel Fuel Using Copper and Nickel Impregnated Activated Carbons. *Energies* **2012**, *5*, 4233−4250.
(64) Cheng, J.; Jin, S.; Zhang, R.; Shao, X.; Jin, M. Enhanced Adsorption Selectivity of Dibenzothiophene on Ordered Mesoporous Carbon-Silica Nanocomposites via Copper Modification. *Microporous Mesoporous Mater.* **2015**, *212*, 137−145.
(65) Haji, S.; Erkey, C. Removal of Dibenzothiophene from Model Diesel by Adsorption on Carbon Aerogels for Fuel Cell Applications. *Ind. Eng. Chem. Res.* **2003**, *42*, 6933−6937.
(66) Fayazi, M.; Taher, M. A.; Afzali, D.; Mostafavi, A. Removal of Dibenzothiophene Using Activated Carbon/γ-Fe_2O_3 nano-Composite: Kinetic and Thermodynamic Investigation of the Removal Process. *Anal. Bioanal. Chem. Res.* **2015**, *2*, 73.
(67) Farzin Nejad, N.; Shams, E.; Amini, M. K.; Bennett, J. C. Synthesis of Magnetic Mesoporous Carbon and Its Application for Adsorption of Dibenzothiophene. *Fuel Process. Technol.* **2013**, *106*, 376−384.

DOI: 10.1021/acsomega.9b03432
ACS Omega 2019, 4, 20844−20853